INSTITUTE OF PHYSICS PUBLISHING MEASUREMENT SCIENCE AND TECHNOLOGY

Meas. Sci. Technol. **16** (2005) 1945–1953 doi:10.1088/0957-0233/16/10/009

Use of bubble image velocimetry for measurement of plunging wave impinging on structure and associated greenwater

Yonguk Ryu, Kuang-An Chang and Ho-Joon Lim

Department of Civil Engineering, Texas A&M University, College Station, TX 77843-3136, USA

Received 10 December 2004, in final form 14 April 2005
Published 23 August 2005
Online at stacks.iop.org/MST/16/1945

Abstract

The measurement of velocity fields of a plunging wave impacting on a structure in a two-dimensional wave tank was investigated experimentally. As the wave impinged and overtopped the structure, a large highly aerated region was created in front of the structure and on top of the structure. The broken wave in front of the structure and associated greenwater on top of the structure are highly aerated containing not only a large number of bubbles but also very large sizes of bubbles. The highly aerated bubbly flow caused the traditional particle image velocimetry (PIV) technique to fail due to the uncontrollable scattering of laser light. A modified PIV method, called bubble image velocimetry (BIV), was introduced by directly using bubbles as the tracer and measuring the bubble velocity by correlating the 'texture' of the bubble images. No laser light sheet was needed while the depth of field was limited to minimize the error. Velocity measurements using BIV and fibre optic reflectometer were compared to validate the BIV technique. While the fluid velocity in the region where no or few bubbles exist can be successfully obtained using PIV, the velocity in the high void fraction region can be measured using BIV. Therefore, BIV can be seen as a complementary technique for PIV. The use of BIV is essential in the studied problem here due to the fact that in the vicinity of the structure the flow is almost entirely bubbly flow. From both the PIV and BIV measurements, it was found that the maximum fluid particle velocity as well as the bubble velocity in front of the structure during the impinging process is about 1.5 times the phase speed of the waves.

Keywords: velocity measurement, multiphase flow, wave breaking, particle image velocimetry, wave–structure interaction

1. Introduction

It is well known that extreme waves have caused significant damage to offshore structures due to the tremendous forces created by wave impingement (e.g., Buchner (1995), Hamoudi and Varyani (1998), Schoenberg and Rainey (2002)). Frequently, the impinging waves rush upward to the deck and create so-called greenwater on the deck that washes out and damages equipment and, in some cases, causes injury or death to persons working on the deck. One recent example is the greenwater damage caused by Hurricane Ivan in the Gulf of Mexico in 2004 that damaged several offshore platforms.

The interaction of extreme waves and structures has been studied for decades. Typically large breaking waves were used to represent the extreme waves. The focus of the studies has been on the forces of the waves on structures and flow field kinematics. While many studies were carried out using numerical models, most of the models were based on the potential flow theory, therefore the multiphase highly turbulent flow in the problem was not realistically simulated. The results were therefore for the 'engineering use' for

prediction of wave forces rather than looking for physical insight of the phenomenon. On the other hand, more advanced approaches, either based on the Reynolds averaged Navier–Stokes equations (RANS) or large eddy simulation (LES), that feature turbulent models and provide much more physical insight have started to be used in the study (e.g., Lin and Liu (1998a, 1998b), Watanabe and Saeki (1999), Christensen and Deigaard (2001)). However, limited success was achieved due to the lack of comprehensive treatments on the splashing free surface and the high void fraction bubbly flow, and lack of experimental data to validate the calculations and the models.

Since very few non-intrusive quantitative velocity measurements of breaking waves impinging on structures exist, we thus review the measurement of breaking waves instead. The measurement on breaking waves itself has been of great interest to numerous researchers. Various measurement techniques, including laser Doppler velocimetry (LDV) and particle image velocimetry (PIV), have been employed for the velocity measurements of the wave breaking process in both the surf zone and deep water (e.g., Greated and Emarat (2000), Ting and Kirby (1994, 1995), Perlin *et al* (1996)). Among the efforts, PIV is a newcomer and only about ten years old. However, the technique is perhaps the most robust and state-of-the-art technique among all the methods. This is due to not only its full field nature but also its recent advances in the improvement of the spatial and temporal resolution and time resolving capability, and its still-evolving foreseeable future.

Among the recent advances in breaking wave measurement using PIV, Chang and Liu (1998) measured the maximum velocity and associated acceleration and vorticity of the overturning jet of a breaking wave. Unfortunately, as a wave breaks and entrains air bubbles, the technique is then restricted to the region outside the aerated area, in general under the trough level or away from the breaking point. Despite some success on the measurement of the breaking wave flow field and generated turbulence outside the aerated region (Chang and Liu 1999, 2000, Melville *et al* 2002), advances in the understanding of the flow structure inside the highly aerated region have rarely been reported. The few exceptions are perhaps the early work of Jansen (1986) and the very recent work of Govender *et al* (2002). Jansen measured particle trajectories in the aerated region of breaking waves using fluorescent tracers and ultraviolet light, but the measurements suffered from poor spatial resolution. More comprehensive measurements were obtained by Govender *et al* (2002), who used a technique similar to PIV based on digital image acquisition and cross-correlation algorithms with the use of a laser light sheet to illuminate the aerated region. Bubble structures in the images were used for correlation between consecutive images for velocity determination. Even though the measurements are promising, no detailed description on the technique itself was provided.

In addition to the direct measurement of bubbly flow under breaking waves, the measurement of gas–liquid flows has been investigated in various areas. Typically the bubble void fraction and the bubble size are much lower and smaller than those in a breaking wave. For such flows the scattering of laser light due to bubbles is much less and thus more controllable. The PIV technique has been successfully used to measure bubble velocity by correlating bubbles or tracking each bubble in the recorded images that were taken by applying the 'shadowgraphy' method (Hassan *et al* 1998, Nishino *et al* 2000, Lindken and Merzkirch 2001). The method uses a light source behind the bubbles, therefore the bubbles appear in the images as their shadows. Again, the density and size of bubbles have to be within a certain limit so the shadows are separated and identifiable. Typically the methods are used in low void fraction flow with small bubbles, and may not be applicable in breaking wave measurements.

This paper presents an experimental study on the kinematics of plunging waves impinging and overtopping a structure. The velocity field in the aerated region around the structure that is the most interesting and important to the problem but difficult to measure using PIV was obtained using the bubble image velocimetry (BIV) technique. The BIV technique is similar to PIV except it directly correlates the bubble images and does not require a laser light sheet for illumination. The principle of the BIV method will be described in detail. The velocity fields measured by using both the traditional PIV technique with a laser light sheet and the new BIV method will be compared and discussed. The BIV measurement will be compared with the result using fibre optic reflectometry (FOR) (Chang *et al* 2003) for validation. The sequential velocity field in the vicinity of the structure will be demonstrated.

2. Experimental condition and setup

2.1. Experimental condition

The experiments were performed in a glass-walled wave tank located at the Department of Civil Engineering, Texas A&M University. The wave tank is 36 m long, 0.9 m wide and 1.5 m high. The water depth was kept constant at $h = 0.80$ m throughout the experiments. The wavemaker is of dry-back flap type installed at one end of the wave tank and controlled by a computer. A 1:5.5 sloping beach with a layer of horsehair is at the other end of the tank to absorb the wave energy and reduce reflection. A rectangular model structure that has a length of 0.15 m, a height of 0.31 m and a width the same as that of the tank was installed in the wave tank. The draft of the model structure is 0.20 m. The model was constructed based on a simplified tension-leg platform with a scale ratio of 1:168. The model structure was mounted on aluminium frames that were rigidly fixed to the bottom of the tank and suspended from the top of the tank. The aluminium frames were designed to minimize the vibration of the model structure induced by breaking wave impingement. The sketch of the model structure is shown in figure 1 with the coordinate system and the fields of view (FOV) used for particle image velocimetry and bubble image velocimetry measurements. Note that the origin $(x, z) = (0, 0)$ is at the intersection of the structure front wall and the stationary water level. The structure was located 21.7 m away from the wavemaker. All the control signals, including the signals controlling the wavemaker and triggering the PIV/BIV system, and measured data were synchronized.

The breaking wave tested is a plunging breaker that was generated using a wave focusing method similar to that in

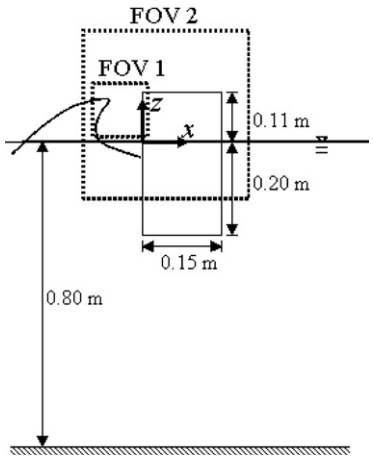

Figure 1. Sketch of the model structure, coordinate system, and fields of view used in PIV and BIV.

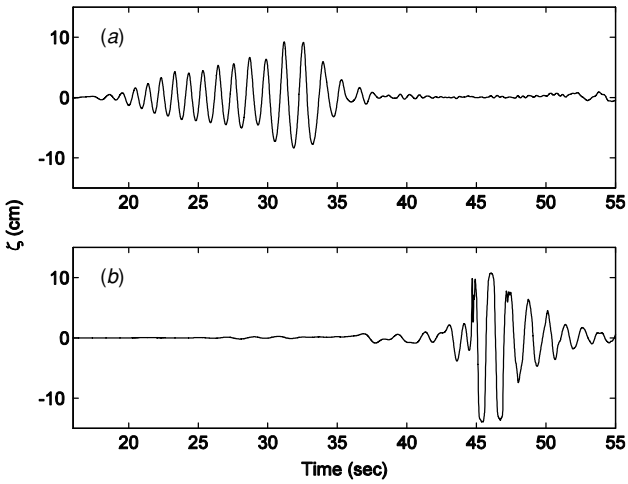

Figure 2. Wave elevations measured at (*a*) 5.1 m ($x = -16.6$ m), and (*b*) 21.7 m ($x = 0.0$ m) from the wavemaker.

Skyner *et al* (1990). The wave train consists of waves with various frequencies ranging from 0.7 Hz to 1.3 Hz. With the superposition of different wave frequencies and some trial and error, the plunging breaker broke at the desired location right in front of the structure. The free surface elevation was measured using two wave gauges located at 5.1 m and 21.7 m from the wavemaker (i.e., $x = -16.6$ m and $x = 0.0$ m in front of the structure) to measure the incoming waves and the water elevation at the front edge of the structure. The measured wave condition is shown in figure 2.

2.2. Setup of PIV system

The PIV technique in the present study was first used to measure the velocity field near the front wall of the model structure. The light source of the PIV system is a dual-head frequency-doubled Spectra-Physics Nd:YAG laser that has a 532 nm wavelength, 400 mJ maximum output energy, 6 ns pulse duration and 10 Hz repetition rate for each head. A set of optics consisting of cylindrical and spherical lenses was used to generate the light sheet. The image recording device is a CCD camera from LaVision Inc. that has an eight frames per second (fps) maximum framing rate, a resolution of 1024 $\times$ 1280 pixels and a 12-bit dynamic range. The seeding particles, Vestosint 2157, have a mean diameter of 56 μm and a specific weight of 1.02. The FOV for the PIV measurements is from $x = -14$ cm to $x = 0.7$ cm and from $z = 1$ cm to $z = 13$ cm with $x = 0$ being the leading edge of the structure and $z = 0$ being the calm water level as shown in figure 1 (denoted as FOV1). The time interval between two successive laser pulses is 0.6 ms. The frame rate was set at 7.27 Hz during all experiments. The measurements were repeated 11 times with a small delay between each so continuous velocity fields with a time interval of 0.025 s were obtained. The interrogation area for velocity determination was 32 $\times$ 32 pixels with a 50% overlap. Commercial software from LaVision was used for the velocity computation.

2.3. Principle and setup of the BIV system

The BIV technique was used to obtain the velocity field in the aerated region. The technique correlates the bubble images and 'texture' in the images created by the bubbles and the air–water interfaces. No small seeding particles as used in the traditional PIV technique are needed. The idea of the BIV method came from combining the shadowgraphy technique that illuminates the fluid from behind to reveal the flow pattern, and the PIV technique that correlates the consecutive images to determine the velocity. Since the velocity is calculated through cross-correlating the images obtained by the shadowgraphy technique with the bubble structure in the images as tracers, the BIV technique requires only two light projectors to illuminate the air bubbles in the aerated region. Unlike the traditional PIV technique, no laser light sheet is needed. In this study, regular 600 W light bulbs with reflecting mounts were used to illuminate the flow. The images were captured by a Phantom high speed camera mounted with a Nikon 105 mm micro focal lens. The camera has a resolution of 512 $\times$ 512 pixels, an 8-bit dynamic range and a maximum framing rate of 1000 fps. The aperture of the camera was set with the *f*-number equal to 1.8.

The illumination of the flow is a modification of the traditional shadowgraphy method with lights being placed at both sides of the wave tank. One light placed at the back side of the tank was used to illuminate the flow from behind (the high speed camera was located on the other side). A thin sheet of translucent white plastic glass was attached to the back-side glass wall of the tank. This way the light bulb will illuminate the flow more uniformly without the use of a costly large high intensity light emitting diode (LED) plate typically used in the shadowgraphy technique. However, for the region with a high concentration of bubbles the captured images will be filled with shadows and appear to be all dark in that region. The images do not provide the needed differences in intensity to reveal the bubble structure or bubble 'texture' for later correlation. To resolve this problem, a light was placed on the other side of tank (on the same side as the high-speed camera but at an angle) in order to produce the desired intensity differences in the images. The light illuminating behind the tank was located at an angle of 0° (normal to the FOV) while that on the other side had an angle of about 60°. Subsequently, images captured using the modified shadowgraphy technique were inverted so high intensity (bright) represents the bubbles.

The flow velocity was calculated by cross-correlating the flow texture from the inverted consecutive images.

Since the BIV technique does not use a light sheet to illuminate a specific plane of interest like the traditional PIV method, it is necessary to know where the measured bubbles are in the cross-tank direction (i.e. the y direction). The problem is solved by limiting the depth of field (DOF) in the experiment, achieved by carefully setting up the camera. The DOF is defined as the distance within which objects captured by the camera are well focused and appear to be sharp. The camera focal point and the DOF can be considered as the light sheet plane and light sheet thickness, respectively, in the PIV technique. This way the FOV of the captured images can be defined. Assuming that a lens focuses on a point at a distance L from the forward nodal point of the lens (which is sufficiently close to the distance between the lens front and the point), the DOF can be calculated using the formulae below. Following Ray (2002), the formulae for the nearest limit, R, and the farthest limit, S, of the DOF can be expressed as $R = Lf^2/(f^2 + NLC)$ and $S = Lf^2/(f^2 - NLC)$, in which f is the focal length of the camera focal lens, C is the value for the circle of confusion that depends on the property of the camera and N is the f-number of the camera aperture. The DOF is $D = S - R$.

Objects located in front of and behind the DOF will appear to be blurred without a clear texture in the captured image and therefore have little effect on the later correlation process for velocity determination. On the other hand, objects located within the DOF will be sharp in the image with a featured pattern due to the flow. This means that the obtained velocity from cross-correlating the captured images is indeed mainly contributed from the image of fluid within the DOF. The uncertainty on the position of the images in the cross-tank direction is therefore one-half of the thickness of the DOF from the centre of the DOF. As a result, the error due to the thickness of the DOF in the obtained velocity can be estimated approximately as $\varepsilon = D/2L$. If the depth of view D is thin and the distance between the camera and the focal plane L is long, the error can be minimized. In the present study, $L = 4.0$ m, $f = 105$ mm, $N = 1.8$ and $C = 0.03$ mm. The calculated R is about 3.92 m and S is about 4.07 m therefore the corresponding DOF in the present study is $D = 0.15$ m. The error due to the thickness of the DOF is estimated as 2%. The arrangement of the BIV system is sketched in figure 3.

The FOV for the BIV measurement is 37.8 cm × 37.8 cm and centred at $x = 5.2$ cm and $z = -5.3$ cm as shown in figure 1 (denoted as FOV2). The time interval between the recorded images was 1.75 ms, which is equal to the time separation between the consecutive frames captured by the high speed camera. The images were processed using the LaVision PIV software and the velocity field was calculated using an adaptive multi-pass algorithm with an initial interrogation window size of 32 × 32 pixels and a final window size of 16 × 16 pixels with a 50% overlap. A median filter was subsequently applied to eliminate the spurious vectors in the calculated velocity map. The mean velocity was calculated from ensemble averaging ten instantaneous velocity fields from repeated runs with the same test condition.

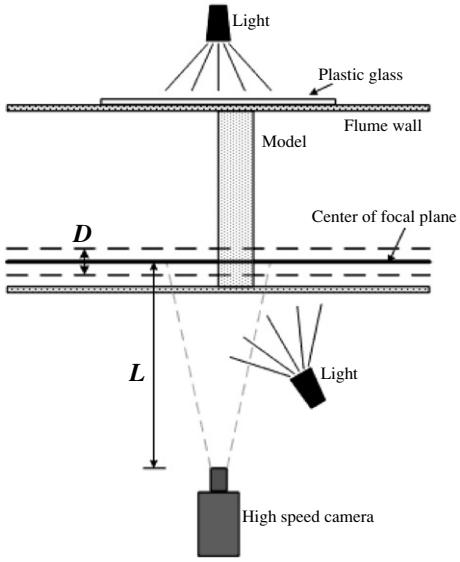

Figure 3. BIV apparatus.

3. Validation of the BIV method

The validation of BIV was performed in two ways: first to compare the velocity measured using the BIV technique with that measured using the fibre optic reflectometry technique; second to check the effect of the blurry images out of the DOF in the BIV velocity measurement. A bubble plume in a water tank was used in the validation.

A two-phase quasi-steady bubbly flow in a vertical narrow tank was measured using both the BIV technique and the FOR technique. The objective of this experiment is to validate the BIV method by comparing the results obtained from these two methods. The FOR technique is capable of measuring the velocity time history of both water (seeded with small particles) and air bubbles at a given point in a multi-phase flow. Details of FOR are given by Chang *et al* (2003).

The vertical narrow tank used in the validation has a length of 0.4 m, a width of 0.4 m and a height of 0.8 m. Water was filled to a depth of 0.7 m in the tank. An air diffuser generating air bubbles was located at the bottom of the tank. A bubble plume was formed in the tank with a diameter approximately 0.11 m at the measurement section. The BIV method was used to measure the velocity of the bubble plume with a FOV of 12.6 cm × 12.6 cm. Subsequently, the FOR technique was employed to measure the velocity at $x_b = 0$ and $z_b = 45$ cm, located in the region of the BIV FOV with $x_b = 0$ and $z_b = 0$ being the centre of the air diffuser. The void fraction is 4% with the average size of a bubble equal to 3 mm at the FOR measurement point, obtained by FOR. Figure 4 shows the measured bubble velocities using both the BIV and FOR methods at the point where the FOR probe was located. The mean velocities were obtained using 20 and 10 instantaneous velocities in the BIV and the FOR measurements, respectively. The comparison of the mean velocities shows very good agreement with a relative error about 1% (approximately 4 mm s^{-1}). The scattering of the instantaneous velocities may be due to the turbulent nature of the flow.

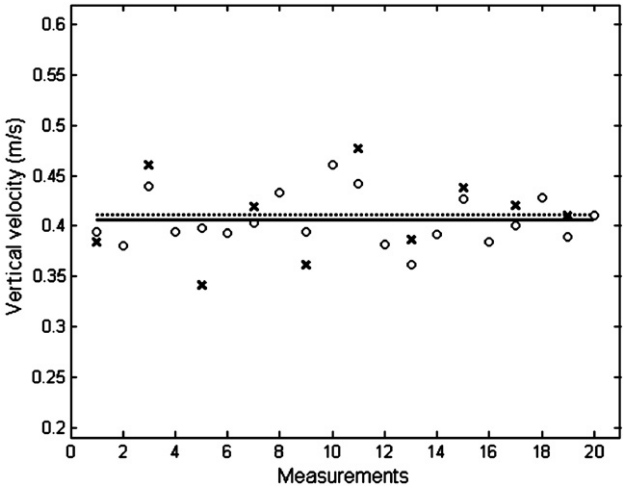

Figure 4. Comparison of velocities by BIV and FOR measurements: 'o', BIV instantaneous velocities; '×', FOR instantaneous velocities; solid line, BIV mean velocity; dotted line, FOR mean velocity.

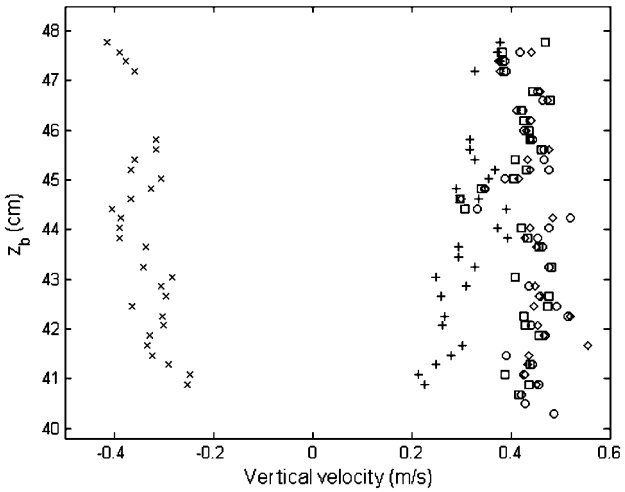

Figure 5. Velocity distribution along the centreline of the bubble plume obtained from: clear images (o), blurry images (+), upside down blurry images (×), superimposed clear and blurry images (□), superimposed clear and flipped blurry images (◊).

In theory the blurred images contributed from bubbles outside the DOF are expected to have insignificant influence in the correlation for velocity determination because the intensity of the bubbles is much weaker (and spread wider) than that of the well-focused bubbles inside the DOF. Since typical BIV measurements are performed in highly aerated bubbly flows, the captured images are indeed the sharp images inside the DOF superimposed with blurry images outside the DOF. In order to investigate the blurry image effect on the BIV accuracy, the velocity obtained from clear bubble images was compared with that obtained from artificially superimposed blurry bubble images. One set focused at the centre of the bubble plume so the bubble images are sharp and clear, while another set focused 15 cm behind the centre of the plume therefore the bubble images are blurred and out of focus. Both sets of original images were processed with velocities obtained.

Clear and blurry images were then artificially added in two ways. Firstly, the blurry images were added to the clear images directly. Secondly, the blurry images were vertically flipped and then added to the clear images. Figure 5 shows the instantaneous vertical velocity distribution obtained along the centreline of the bubble plume from the clear images, blurry images, vertically flipped blurry images, the superposition of the clear images and blurry images, and the superposition of the clear images and vertically flipped blurry images. The figure shows that both the velocities obtained from the clear–blurry superimposed images are very close to that from the clear images. Therefore, the blurry and out of focus bubble images have little effect on the accuracy of the BIV velocity measurement.

4. Results and discussion

The velocity measurement in the vicinity of the model structure was first carried out using the PIV technique. For the spilling type of breaking waves impinging on the structure, the air pocket between the wave front face and the structure is relatively small therefore the majority of the region in front of the leading edge of the structure is not highly aerated and suitable for PIV. However, even for the cases with only a small air pocket, greenwater above the structure due to overtopping is highly aerated and not ideal for PIV. If the impinging wave is of plunging type, a large air pocket in front of the structure will form and cause severe light scattering and result in saturated and not useful images for PIV correlation. The problem continues to the greenwater on top of the structure. Figure 6 shows the PIV measurement of the plunging breaking wave taken at FOV1 shown in figure 1. Clearly there exists a large region where no velocity vectors were obtained due to the large amount and size of air bubbles. A similar problem was also observed in Chang and Liu (1999, 2000). One thing we would like to point out is that the maximum magnitude of the velocity in figure 6(*a*) reached 1.5 times the phase speed of the wave. This result is consistent with that reported in Chang and Liu (1998).

The BIV technique uses the bubbles as tracers and correlates the bubble texture in the aerated region. This means that the BIV technique works in the region where the PIV technique does not work. Figure 7 shows a sample of inverted BIV images captured for the present study. The flow pattern of the bubble in front of the structure and the splashing jet above the structure are clearly identified in the image. Figure 8(*a*) shows the image and texture in the aerated region that is a close-up of figure 7 (see the marked area in the figure) without image inversion. Since the air bubbles appeared to be dark, the image was inverted, as shown in figure 8(*b*), before performing correlation for velocity determination. Figure 8(*c*) shows the obtained BIV velocity vectors through cross-correlating the inverted images. As a result, it is shown that as long as there exists a certain amount of air bubbles or air–water interfaces that form a distinct flow pattern or texture in the images, velocities can be obtained by cross-correlating the images.

Figure 9 shows the velocity field under the same experimental condition as in figure 6 but measured using the BIV technique. The field of view is shown in figure 1

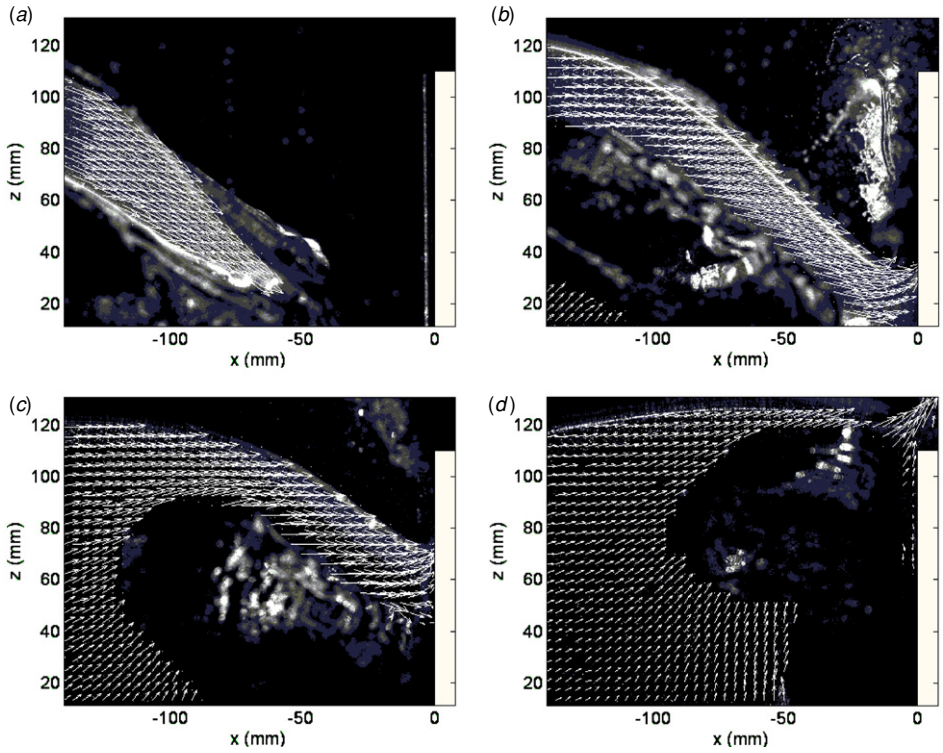

Figure 6. PIV measurement of plunging breaking wave impinging on structure. The time separation between the panels is 25 ms.

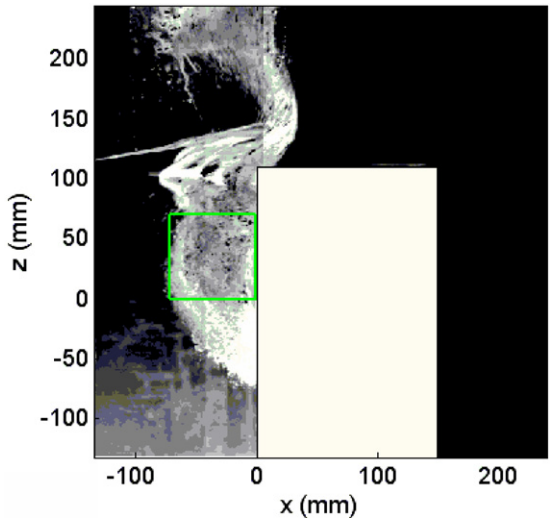

Figure 7. Sample BIV image of wave impinging on structure.

and denoted as FOV2. The entire sequence of the velocity field during the impinging and greenwater processes is demonstrated in the figure. Note that the velocity field is the mean velocity obtained from ensemble averaging ten repeated instantaneous BIV velocity measurements while the images were picked from one of the ten realizations (i.e., the images are instantaneous). Since the wave breaking process is highly turbulent, the instantaneous images do not match the mean velocities perfectly in some instants. $t = 0$ in the figure represents the instant when the overturning jet of the breaking wave touched the front water surface before impinging on the structure.

Figure 9(a) shows the moment right after the overturning jet touched its front water surface and before it touched the front wall of the structure. The jet velocity is moving downstream and downward. After a short duration of 35 ms in figure 9(b), the overturning wave impinged the structure's frontal wall and splashed upward. At this moment a large part of wave was still moving horizontally towards the structure while the splashing jet was moving vertically. The process continued to figure 9(c) until the wave momentum pushed the wave front to move forward onto the deck, as shown in figure 9(d). At the same time, when the wave momentum pushed part of the water to move upward, it also pushed part of the water to move downward and created a large vortex at around $z = 0$, starting in figure 9(c). The upward greenwater (i.e., water above the deck) did not touch the deck surface until the instant in figure 9(e). The horizontal velocity on the deck was small initially until the water started to touch the deck. In figures 9(f), (g) the greenwater lost its vertical momentum and the velocity became completely horizontal. This could create a large horizontal force exerting on any objects located on the deck due to the large horizontal momentum of water. Since the deck is not long, the greenwater on top of the deck passed the deck and moved downward back to the 'ocean' quickly at the rear edge of the deck. The velocity of the greenwater continued to move downstream but started to change to the downward direction as seen in figures 9(h), (i). After this moment the greenwater quickly receded and lost its momentum with the velocity being significantly reduced, as seen in figures 9(j)–(l).

We would like to point out that the measured velocity using BIV in figure 9 is indeed mainly the bubble velocity for the highly aerated region in front of the structure, and the

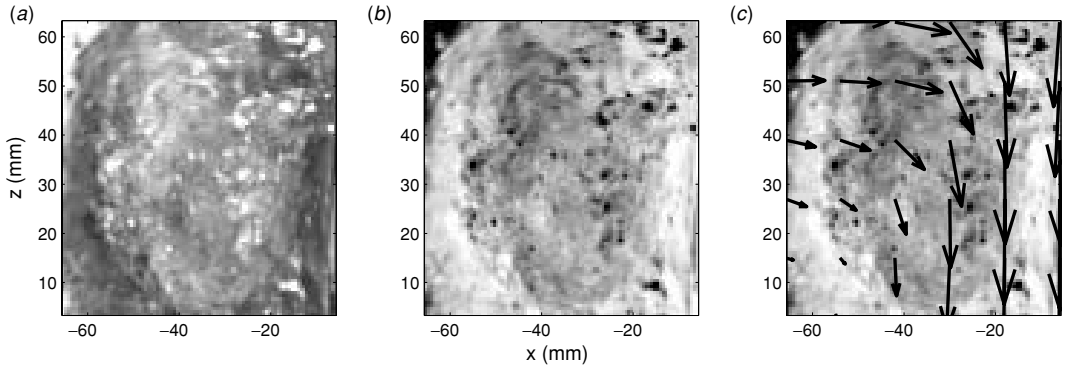

Figure 8. Close-up of the bubbly flow in figure 7 and associated velocity vectors obtained using BIV. (*a*) Raw image, (*b*) inverted image, (*c*) instantaneous velocity field.

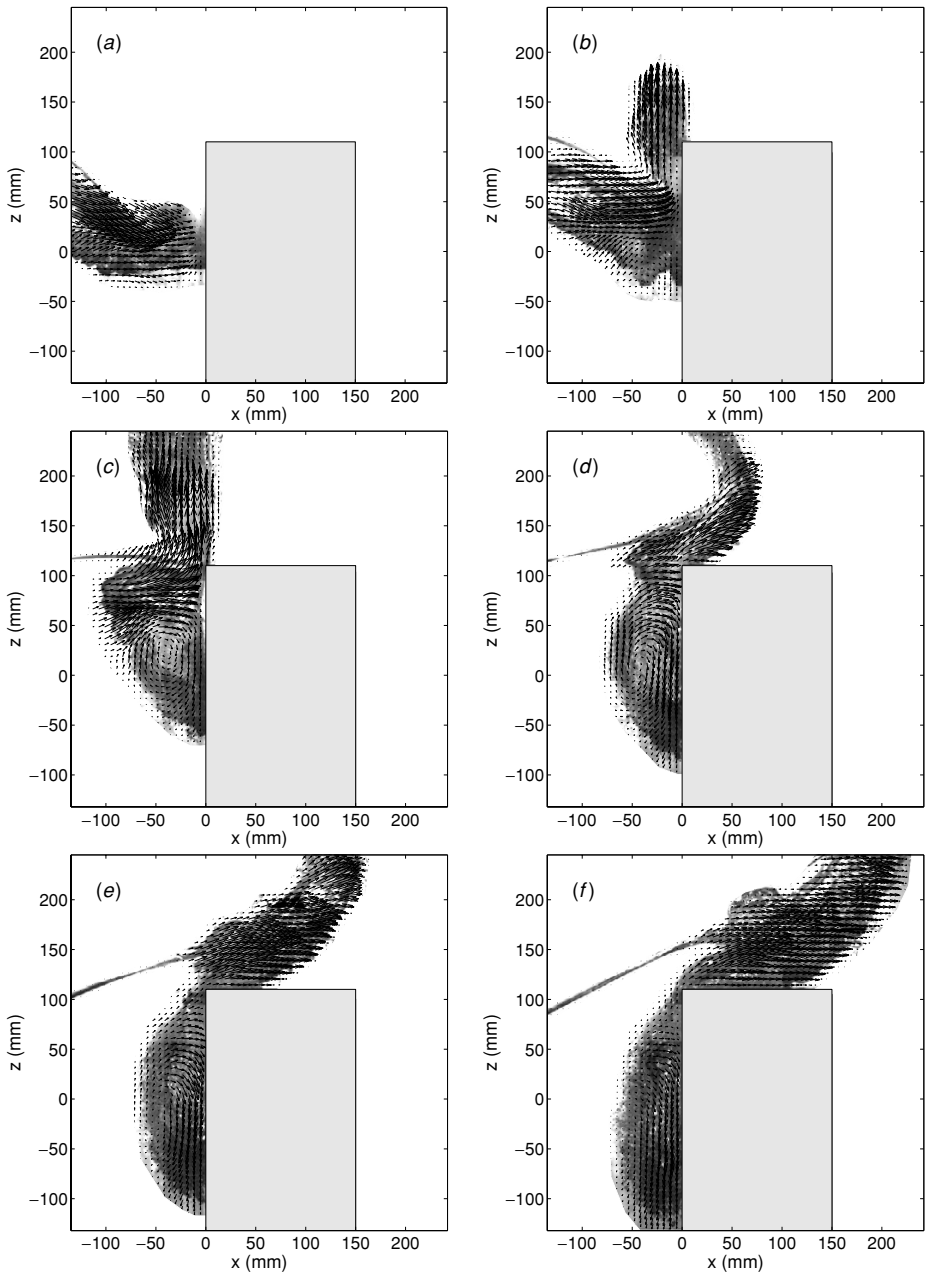

Figure 9. BIV measured mean velocity fields of plunging breaking wave impinging on structure. $t =$ (*a*) 0.022 s, (*b*) 0.057 s, (*c*) 0.092 s, (*d*) 0.127 s, (*e*) 0.162 s, (*f*) 0.197 s, (*g*) 0.232 s, (*h*) 0.267 s, (*i*) 0.302 s, (*j*) 0.337 s, (*k*) 0.372 s and (*l*) 0.507 s.

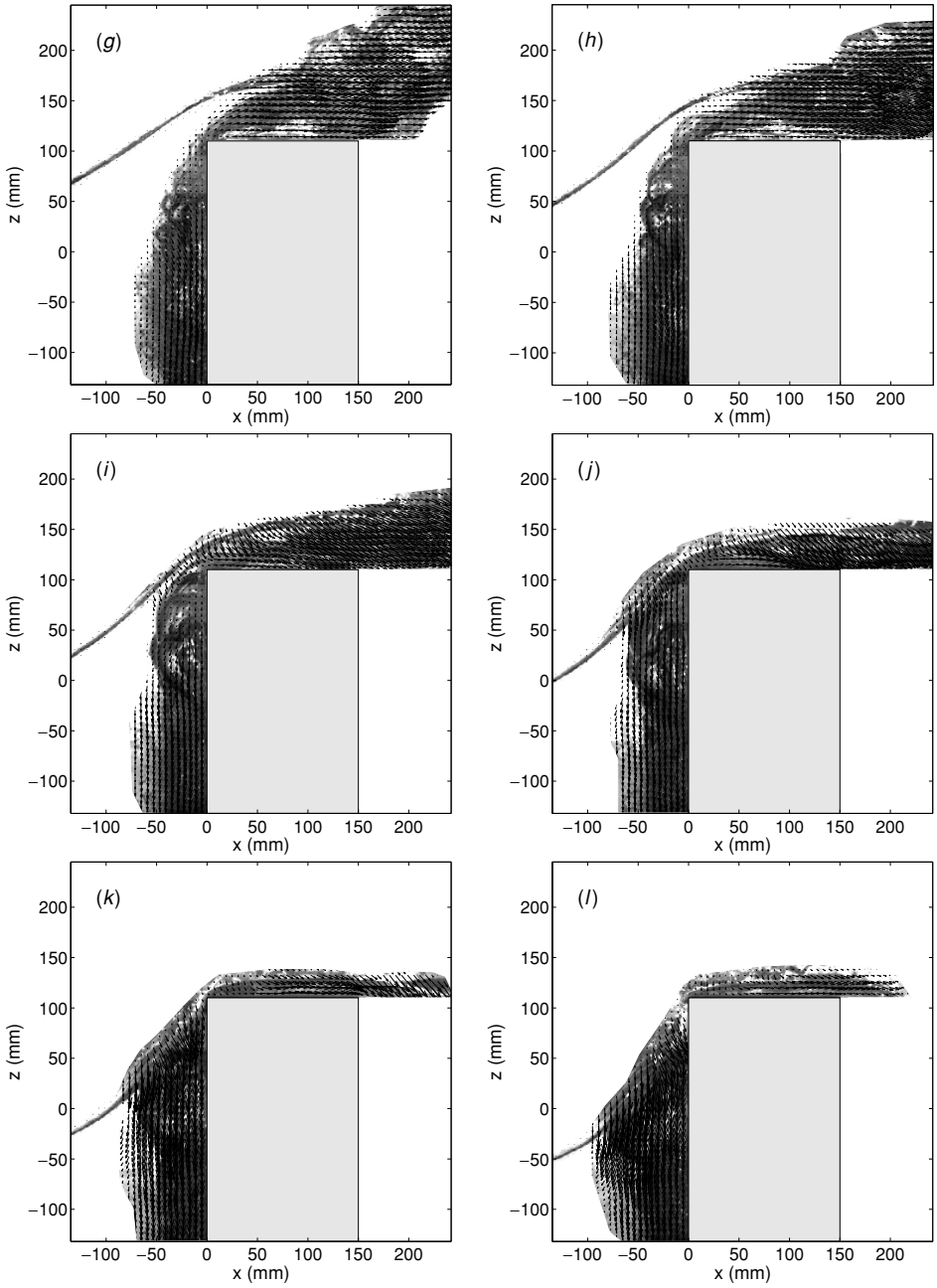

Figure 9. (Continued.)

fluid (air–water mixture) velocity above the structure deck. While we are more confident on the measured greenwater velocity above the deck due to the relatively minor effect of the buoyant force on the inertial force in that region, we are not sure whether the fluid velocity followed the air bubble velocity in the aerated region in front of the structure. The buoyant force may be significant in that region due to the relative low fluid velocity. This is especially true when large air bubbles were generated at certain phases. From the images captured by the fast speed camera, the bubble size reached nearly 5 cm in diameter during the period between figures 9(*i*) and (*j*). More studies are needed to clarify the differences between the velocity of air bubbles and that of water.

5. Summary and conclusion

The measurements of the velocity fields of a plunging breaking wave impinging on a structure and the associated greenwater above the structure using the PIV and BIV techniques were presented. While the PIV technique was only capable of obtaining the velocity field outside the aerated region in front of the structure, the BIV technique successfully measured the velocity field of the greenwater and the aerated region of the breaker. The BIV technique is indeed a modified PIV technique with images captured based on a modified shadowgraphy technique. The technique does not require the use of a laser thus has a much lower cost and is easier to set up. The BIV technique was validated by comparing the

velocity measured using the FOR method. The BIV technique measures velocity mainly in the multiphase region where the PIV technique does not work well or does not work at all. The technique therefore can be considered as a complementary technique for PIV in the study of high void fraction multiphase flows such as breaking waves.

Acknowledgments

The authors wish to thank the financial support in part from the Minerals Management Service and in part from the industry funding through the Offshore Technology Research Center (OTRC) under the project entitled 'Mitigating Greenwater Damage through Design'. Special thanks go to Dr Richard Mercier, Director of OTRC, for his support and input.

References

Buchner B 1995 The impact of green water on FPSO design *Offshore Technology Conf. 95 OTC* 7698 pp 45–57

Chang K-A, Lim H-J and Su C B 2003 Fiber optic reflectometer for velocity and fraction ratio measurements in multiphase flows *Rev. Sci. Instrum.* **74** 3559–65

Chang K-A and Liu P L-F 1998 Velocity, acceleration and vorticity under a breaking wave. *Phys. Fluids* **10** 327–9

Chang K-A and Liu P L-F 1999 Experimental investigation of turbulence generated by breaking waves in water of intermediate depth *Phys. Fluids* **11** 3390–400

Chang K-A and Liu P L-F 2000 Pseudo turbulence in PIV breaking-wave measurements. *Exp. Fluids* **29** 331–8

Christensen E D and Deigaard R 2001 Large eddy simulation of breaking waves *Coast. Eng.* **42** 53–86

Govender K, Mocke G P and Alport M J 2002 Video-imaged surf zone wave and roller structures and flow fields *J. Geophys. Res.* **107** 3072

Greated C A and Emarat N 2000 Optical studies of wave kinematics *Advances in Coastal and Ocean Engineering* vol 6 ed P L-F Liu (Singapore: World Scientific) pp 185–223

Hamoudi B and Varyani K S 1998 Significant load and green water on deck of offshore units/vessels. *Ocean Eng.* **25** 715–31

Hassan Y A, Schmidl W D and Ortiz-Villafuerte J 1998 Investigation of three-dimensional two-phase flow structure in a bubbly pipe *Meas. Sci. Technol.* **9** 309–26

Jansen P C M 1986 Laboratory observations of the kinematics in the aerated region of breaking waves *Coast. Eng.* **9** 453–77

Lin P and Liu P-F 1998a A numerical study of breaking waves in the surf zone *J. Fluid Mech.* **359** 239–64

Lin P and Liu P-F 1998b Turbulence transport, vorticity dynamics, and solute mixing under plunging breaking waves in surf zone *J. Geophys. Res.* **103** 15677–94

Lindken R and Merzkirch W 2001 A novel PIV technique for measurements in multi-phase flows and its application to two-phase bubbly flows *4th Int. Symp. on Particle Image Velocimetry* paper A 231

Melville W K, Veron F and White C J 2002 The velocity field under breaking waves: coherent structures and turbulence *J. Fluid Mech.* **454** 203–33

Nishino K, Kato H and Torii K 2000 Stereo imaging for simultaneous measurement of size and velocity of particles in dispersed two-phase flow *Meas. Sci. Technol.* **11** 633–45

Perlin M, He J and Bernal L P 1996 An experimental study of deep water plunging breakers. *Phys. Fluids* **8** 2365–74

Ray S D 2002 *Applied Photographic Optics* (Oxford: Focal) pp 215–33

Schoenberg T and Rainey R C T 2002 A hydrodynamic model of green water incidents *Appl. Ocean Res.* **24** 299–307

Skyner D J, Gray C and Greated C A 1990 A comparison of the time-stepping numerical predictions with whole-field flow measurement in breaking waves *Water Wave Kinematics* ed A Torum and O T Gudmestad (Boston: Kluwer) pp 491–508

Ting F C K and Kirby J T 1994 Observation of undertow and turbulence in a laboratory surf zone *Coast. Eng.* **24** 51–80

Ting F C K and Kirby J T 1995 Dynamics of surf-zone turbulence in a strong plunging breaker *Coast. Eng.* **24** 177–204

Watanabe Y and Saeki H 1999 Three-dimensional large eddy simulation of breaking waves *Coast. Eng. J.* **41** 281–301